THE JOURNAL OF PHYSICAL CHEMISTRY LETTERS
A JOURNAL OF THE AMERICAN CHEMICAL SOCIETY

pubs.acs.org/JPCL Letter

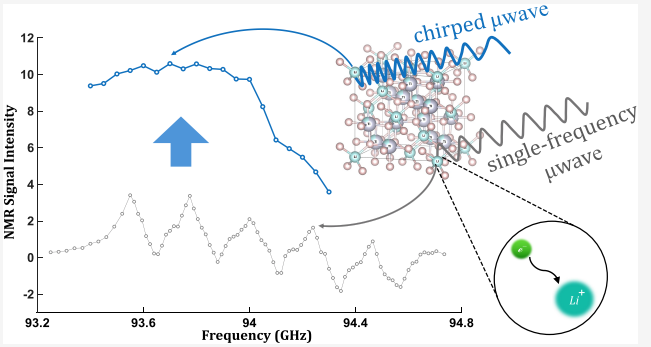
Coherent Pulsed Dynamic Nuclear Polarization with Endogenous Metal Ions

Liangping Zhu, Duhan Zhang, Haoyu Liu, Ashley N. Beers, Yunfan Qiu, Thierry Dubroca, and Yifan Quan*

Cite This: *J. Phys. Chem. Lett.* 2026, 17, 10613−10621 Read Online

ACCESS | Metrics & More | Article Recommendations | Supporting Information

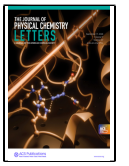
ABSTRACT: Dynamic nuclear polarization (DNP) can overcome the intrinsically low sensitivity of nuclear magnetic resonance (NMR) and enable structural characterization of a wide range of materials. In inorganic solids, DNP can be achieved endogenously by introducing paramagnetic metal ions as polarizing agents directly into the host lattice. However, DNP enhancements obtained with metal ions are typically an order of magnitude lower than those achieved with organic radicals because of the intrinsic properties of high-spin metal-ion electron systems. Here, we present the first experimental demonstration of coherent pulsed endogenous metal-ion DNP using frequency-swept chirped microwave excitation at the W-band (94 GHz). Experiments on Mn(II)- and Gd(III)-doped $Li_4Ti_5O_{12}$ (LTO) show that the integrated solid effect (ISE) improves DNP efficiency by up to an order of magnitude compared with the conventional single-frequency solid effect (SE). Furthermore, ISE outperforms the adiabatic solid effect (ASE) for these systems with electron paramagnetic resonance (EPR) spectra that are much broader than the nuclear Larmor frequency, in contrast to the behavior observed for narrow-line organic radicals. Frequency-swept excitation is highly robust and maintains near-optimal performance over wide microwave frequency and magnetic field ranges. We further demonstrate that adiabatic microwave pulses can selectively excite the satellite transitions of high-spin electron systems, increasing the population difference of the central transition and thereby providing an additional mechanism for enhancing the DNP efficiency. These results establish coherent frequency-swept pulsed DNP as an effective strategy for overcoming the limitations of endogenous metal-ion DNP and pave the way for highly sensitive NMR studies of inorganic materials.



Dynamic nuclear polarization (DNP) has emerged as a powerful and widely applicable technique for overcoming the intrinsic sensitivity limitations of nuclear magnetic resonance (NMR). Upon microwave irradiation, spin polarization is transferred from the highly polarized unpaired electron spins of a polarizing agent to nearby nuclear spins, increasing NMR signal intensities by several orders of magnitude.[1−3] The resulting sensitivity enhancement has enabled NMR investigations that would otherwise be impractical, including studies of complex biological systems,[4−17] the characterization of materials,[18−29] and magnetic resonance imaging (MRI) through dissolution DNP.[30−32]

In typical DNP experiments, a solid is impregnated with a solution containing radicals that forms a glassy matrix, e.g., glycerol/water or tetrachloroethane (TCE). Electron spin polarization is first transferred from the radicals in the matrix to nuclear spins at or near the sample surface and subsequently propagates into the bulk through nuclear spin diffusion. As a result, this approach can provide direct access to the structure, dynamics, and interactions of a material interface.[18,22,28,33,34] As an alternative to using organic radicals in a glassy matrix, high-spin transition-metal ions such as Gd^{3+} and Mn^{2+} can provide the unpaired electrons required for DNP.[35−38] In this approach, the paramagnetic metal ions can be incorporated directly into the structure of inorganic or molecular solids, known as endogenous metal-ion DNP. Electron polarization is then transferred from paramagnetic centers distributed within the material rather than from exogenous radicals, providing bulk-sensitive signal enhancement. This approach has enabled studies of a wide range of materials, including metal oxides, metal−organic frameworks, perovskites, and semiconductor nanocrystals.[24,28,29,34,36,37,39−41] Endogenous metal-ion DNP also eliminates the need for sample impregnation with a glassy matrix, thereby avoiding undesirable interactions with the solvent or polarization agent and preserving the integrity of the sample, which is crucial for highly reactive materials. In

Received: July 14, 2026
Revised: August 28, 2026
Accepted: September 1, 2026
Published: September 4, 2026



ACS Publications © 2026 American Chemical Society

https://doi.org/10.1021/acs.jpclett.6c02353
J. Phys. Chem. Lett. 2026, 17, 10613−10621

Downloaded from pubs.acs.org/jpclcd/article-pdf/17/37/10613/6838270/acs.jpclett.6c02353.pdf by FLORIDA STATE UNIV user on 02 November 2026

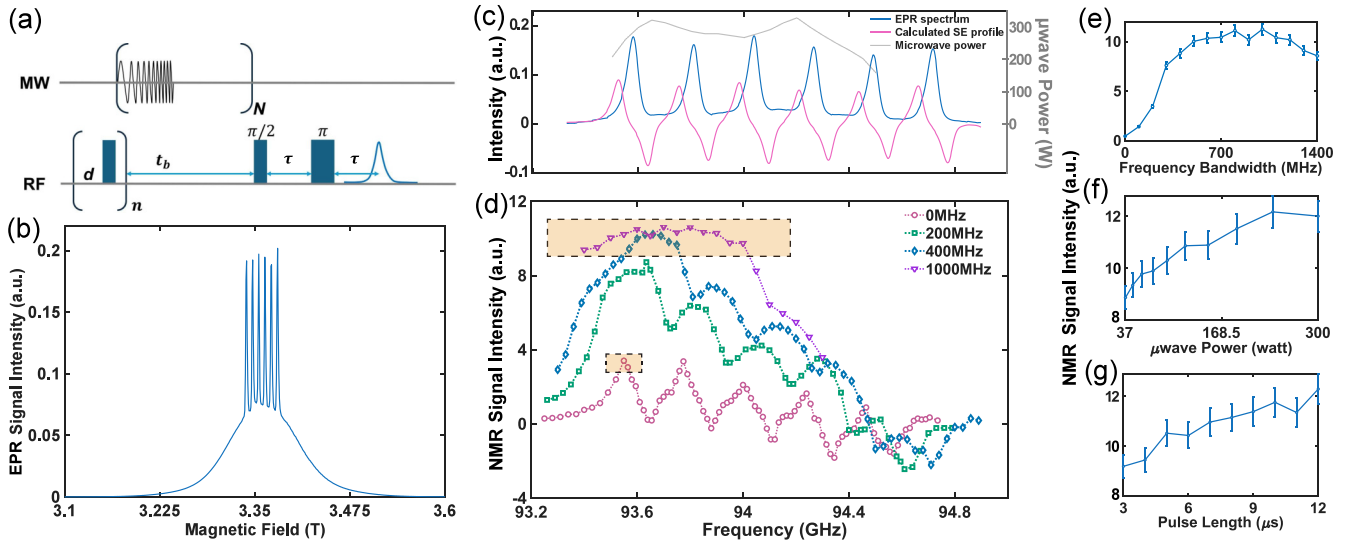


Figure 1. ^{7}Li DNP profiles of Mn-doped LTO. (a) Pulse sequence used for the pulsed DNP experiments. The nuclear polarization was first saturated using a train of RF pulses. Microwave pulses were then applied to transfer electron spin polarization to the ^{7}Li nuclei, and the resulting nuclear polarization was detected by NMR using a Hahn echo sequence. (b) 94 GHz EPR spectrum of Mn-doped LTO sample at 20 K measured with echo-detected field sweep (EDFS). The six narrow peaks correspond to the hyperfine-split central transition, while the broad line is from overlapping satellite transitions. (c) EPR central transition and calculated SE profile, both obtained using panel b as well as the EIK profile. (d) DNP frequency profiles acquired using single-frequency SE (0 MHz chirp) and frequency-swept chirped pulses with frequency bandwidths of 200, 400, and 1000 MHz. The magnetic field was kept at 3.364 T, the third from the right on the EPR spectrum in panel b. The optimal microwave frequencies for ISE and SE are highlighted, illustrating the robustness of ISE. (e) Dependence of the NMR signal intensity on the chirp bandwidth with the initial frequency fixed at 93.3 GHz. (f) Dependence of the NMR signal intensity on the microwave (μwave) power. (g) Dependence of the NMR signal intensity on the microwave pulse length.

addition, paramagnetic metal ions are already widely employed as dopants in functional inorganic materials, where they modify properties such as ionic conductivity, catalytic activity, and optical behavior.[25,29] These paramagnetic dopants can simultaneously serve as polarization agents. Combining endogenous metal-ion DNP with surface-sensitive DNP techniques enables spatially selective NMR investigations by distinguishing between bulk and surface environments.[28,34]

Although metal-ion DNP offers unique opportunities for the structural characterization of materials, its efficiency is often an order of magnitude lower than that achieved with organic radicals,[29,34,36,42,43] thereby limiting its broader application. This limitation arises from the broad electron paramagnetic resonance (EPR) line widths associated with large zero-field splitting (ZFS) and strong hyperfine interactions, as well as the typically rapid electron spin relaxation of paramagnetic metal ions. This limitation becomes even more pronounced at high magnetic fields required for high-resolution NMR because the efficiency of conventional continuous-wave (CW) DNP mechanisms, such as the solid effect (SE) and cross-effect (CE), decreases considerably at high fields due to their inherent field dependence.

Recent advances in coherent pulsed DNP have demonstrated the potential to overcome many of these limitations and significantly improve DNP performance. Unlike CW DNP, pulsed methods exploit precise control of the microwave frequency, phase, and amplitude to manipulate electron spin coherence, thereby mitigating the unfavorable magnetic field dependence of conventional DNP mechanisms and enabling substantially larger enhancements at high fields.[44−57] A prominent example is the recent demonstration of a record DNP enhancement of $\varepsilon \approx 496$ at 94 GHz, approaching the theoretical maximum, using trityl radicals and chirped microwave pulses.[54]

However, most pulsed DNP methodologies have been developed exclusively for mono- and biradical polarizing agents at low magnetic fields, primarily at X- and Q-band frequencies. Here, we report the first experimental demonstration of coherent pulsed DNP using endogenous metal ions in inorganic solids at W-band frequency. By employing chirped microwave excitation, in which the microwave frequency is swept over a defined frequency range during the pulse, we achieve a 3-fold increase in DNP enhancement relative to conventional single-frequency irradiation for Mn^{2+} and a 10-fold increase for Gd^{3+}. These improvements are significantly more pronounced for metal-ion polarizing agents compared to organic radicals,[54] as the broad EPR spectra of metal ions make single-frequency excitation intrinsically inefficient. We compared two chirped DNP regimes: the adiabatic solid effect (ASE), which employs a narrow frequency chirp around a single SE transition, and the integrated solid effect (ISE), which uses a broad chirp spanning both SE transitions (Figure 2).[53] In contrast to narrow-line radicals, for which the ASE has been shown to provide the largest DNP enhancements, we find that the ISE is substantially more efficient for broad-line metal centers where the EPR line width is much broader than the nuclear Larmor frequency. Additionally, we demonstrate that frequency-chirped DNP is robust over a wide range of experimental conditions, providing a practical and effective strategy for efficient polarization transfer in endogenous metal-ion DNP. Finally, we demonstrate that exciting the satellite transitions of high-spin electron systems can enhance the population difference between the states for the central transition $\left(\left|m_S = -\frac{1}{2}\right\rangle \rightarrow \left|m_S = \frac{1}{2}\right\rangle\right)$, providing an additional mean to further improve DNP performance.

https://doi.org/10.1021/acs.jpclett.6c02353
J. Phys. Chem. Lett. 2026, 17, 10613−10621

Downloaded from pubs.acs.org/jpclcd/article-pdf/17/37/10613/6838270/acs.jpclett.6c02353.pdf by FLORIDA STATE UNIV user on 02 November 2026

Mn-doped and Gd-doped $Li_4Ti_5O_{12}$ (LTO) in the form of $Li_{4-x/3}Ti_{5-2x/3}Mn_xO_{12}$ and $Li_{4-x/3}Ti_{5-2x/3}Gd_xO_{12}$, where x = 0.005, were prepared by solid-state reaction for the DNP experiments.[58] Details of the sample synthesis and characterization are provided in sections I and II of the Supporting Information. The experiments were carried out using the recently upgraded W-band high-power quasi-optical EPR spectrometer (HiPER)[59−61] at National High Magnetic Field Laboratory (NHMFL) in Tallahassee, Florida, USA. The spectrometer is equipped with a kilowatt extended interaction klystron (EIK) amplifier (power profile given in the Supporting Information) and a Keysight M8190A arbitrary waveform generator (AWG) allowing the manipulation of the microwave pulses. Samples were cooled using an Oxford Instruments variable-temperature insert (VTI), allowing measurements at temperatures down to 1.3 K. The SpecMan4EPR software package[62] was integrated with the HiPER spectrometer to control the microwave pulse sequences and perform pulsed EPR detection. NMR spectra were recorded using a Tecmag Redstone console in combination with an Agilent 250 W RF amplifier and a home-built saddle-coil RF resonator. Figure 1a illustrates the microwave and RF pulse scheme for the pulsed DNP experiment.

The DNP frequency profiles of the Mn-doped LTO sample, shown in Figure 1d, were measured using single-frequency SE or frequency-chirped ASE/ISE and are compared with the corresponding W-band EPR spectrum. For DNP measurements, the magnetic field was held constant while the microwave frequency was varied using the AWG. Frequency-swept pulses with a duration of 12 μs were applied at a repetition rate of 2 kHz, unless otherwise noted. The frequency sweep bandwidth, microwave power, and pulse length were experimentally optimized, as shown in Figure 1e−g. The optimal microwave power of approximately 200 W (Figure 1f) corresponds to an electron spin nutation frequency ω_1 close to the ^{7}Li nuclear Larmor frequency (55.6 MHz). The high nutation frequency is further confirmed by the electron spin nutation measurement shown in the Supporting Information and ensures coherent manipulation of the electron spin (adiabaticity factor $Q_1 \gg 1$ (vide infra)), which is critical for efficient DNP.[64] Note that, owing to the probe geometry, the microwave field is inhomogeneous across the sample and the experimentally determined optimum represents an average condition that maximizes the overall DNP enhancement. Under single-frequency SE excitation (0 MHz chirp width), the signature multipeak Mn^{2+} DNP frequency profile is observed. Owing to the limited bandwidth (~1 GHz) of the EIK source, the highest-frequency feature could not be fully recorded.

Introducing frequency sweeps significantly increases the DNP enhancement by a factor of approximately 3 compared to single-frequency SE excitation. This relative improvement substantially exceeds that reported for trityl-based pulsed DNP,[54] highlighting the greater benefit of frequency-swept excitation for metal-ion systems. Two factors contribute to this significant enhancement. First, the frequency sweep excites a substantially larger fraction of the Mn^{2+} EPR spectrum. As a result, a much larger fraction of the electron spin ensemble goes through the DNP matching conditions, where effective electron frequency $\omega_{\text{eff}} = \sqrt{(\omega_{0S} - \omega_m)^2 + \omega_1^2} = \omega_{0I}$ matches nuclear Larmor frequency ω_{0I}, and contributes to the nuclear polarization, as illustrated in Figure 2. ω_{0S} denotes

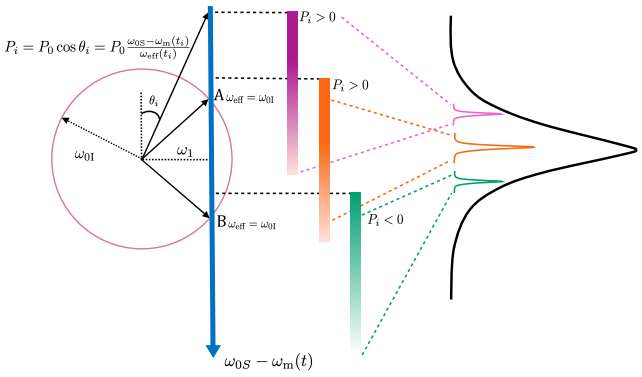


Figure 2. Schematic illustration of frequency-swept pulsed DNP in the rotating frame. During a microwave frequency chirp from $\omega_m(t_i)$ to $\omega_m(t_f)$, the effective frequency (blue trajectory), $\omega_{\text{eff}} = \sqrt{(\omega_{0S} - \omega_m)^2 + \omega_1^2}$, evolves adiabatically. The effective electron polarization, P_i, is determined by the initial microwave frequency and adiabatically follows the effective field. Polarization is transferred to the nuclear spins when either of the two DNP matching conditions (A and B), $\omega_{\text{eff}} = \omega_{0I}$, is satisfied.[53,63] For broad EPR spectra, different electron spin packets (with different ω_{0S} values) have different effective electron polarizations, P_i, which may include both positive and negative values for the same frequency sweep, thereby generating nuclear polarizations of both signs. The resulting nuclear polarizations may partially cancel, reducing the overall DNP enhancement.

the electron Larmor frequency, ω_1 the electron nutation frequency, and ω_m the microwave frequency. This effect is particularly prominent for metal-ion DNP, with much broader EPR than radicals. Second, frequency-swept excitation drives the spin system through Landau−Zener level anti-crossings, enabling more efficient adiabatic polarization transfer than SE.[53,64] Note that when $\omega_1 = \omega_{0I}$, the SE matching condition is satisfied when $\omega_{0S} - \omega_m = 0$, corresponding to the nuclear orientation via electron spin locking (NOVEL) condition.[46,47,65] However, in this case, the electron polarization in the rotating frame is zero (see Figure 2 and the discussion below). This is why NOVEL requires a $\pi/2$ pulse to prepare the electron polarization in the rotating frame before spin locking. When $\omega_1 > \omega_{0I}$, the SE matching condition can no longer be satisfied, leading to a decrease in DNP efficiency as the microwave power is increased.

Comparing different chirped DNP schemes, ISE outperforms ASE, in contrast to previous studies on narrow-line radicals such as trityl, where ASE is typically more efficient.[53,54,66] This performance difference is even more evident for the Gd-doped sample (vide infra). As previously shown,[53] for narrow-line radicals, highly efficient polarization transfer under the first DNP matching condition can result in partial back-transfer of polarization under the second matching condition during the ISE sweep, thereby reducing the net nuclear polarization.

However, the broad EPR spectra of Mn^{2+} (and Gd^{3+}) give rise to a different behavior. During a frequency sweep, the electron magnetization adiabatically follows the effective field. The effective polarization for spin packet S is determined by initial microwave frequency $\omega_m(t_i)$ and nutation frequency ω_1, $P_i = P_0 \cos\theta_i = P_0 \frac{\omega_{0S} - \omega_m(t_i)}{\omega_{\text{eff}}(t_i)}$, with P_0 being the electron polarization and ω_{0S} the Larmor frequency of the spin packet. For a broad ISE sweep initiated sufficiently far from the EPR

https://doi.org/10.1021/acs.jpclett.6c02353
J. Phys. Chem. Lett. 2026, 17, 10613−10621

Downloaded from pubs.acs.org/jpclcd/article-pdf/17/37/10613/6838270/acs.jpclett.6c02353.pdf by FLORIDA STATE UNIV user on 02 November 2026

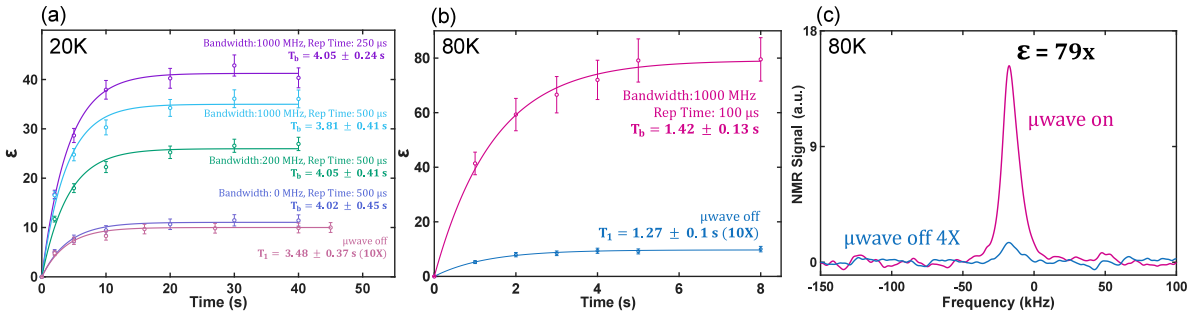


Figure 3. DNP build-up and DNP-enhanced ^{7}Li NMR spectrum of the Mn-doped LTO sample. DNP build-up measured at (a) 20 and (b) 80 K using the optimized experimental parameters (see Figure 1) for different microwave sweep bandwidths. The solid lines are exponential rise fits used to determine the DNP build-up time, T_b. The microwave-off (μwave off) data are multiplied by a factor of 10 for visualization. (c) ^{7}Li NMR spectra acquired at 80 K with (average of 16 scans) and without (average of 512 scans) DNP.

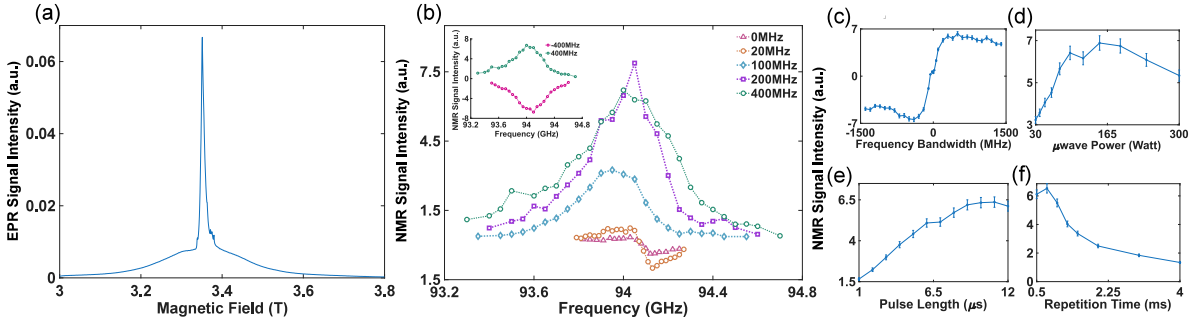


Figure 4. ^{7}Li DNP profiles of the Gd-doped LTO sample. (a) 94 GHz EDFS EPR spectrum of the Gd-doped sample at 20 K. The narrow feature is the central transition, while the broad line is from the satellite transitions. (b) DNP frequency profiles acquired using SE and different frequency-swept chirped pulses. The magnetic field was kept at 3.351 T (EPR peak). The inset compares positive and negative 400 MHz chirps, showing that reversing the chirp direction reverses the sign of the DNP enhancement, demonstrating the coherent nature of chirped DNP. (c) DNP performance as a function of the frequency bandwidth for chirps centered at 94 GHz. (d–f) Dependence of the NMR signal intensity on the microwave power, pulse length, and pulse repetition time, respectively.

spectrum, cos $\theta_i \approx 1$ for essentially all spin packets, so the effective electron polarization is maximized and has the same sign across the entire EPR line. In contrast, the narrower frequency sweeps typically used for ASE can produce opposite effective polarizations (i.e., different signs of P_i) for different regions of the EPR spectrum, leading to partial cancellation of the transferred nuclear polarization, as illustrated in Figure 2. Combined with the fact that the broader ISE sweep affords a much larger fraction of the EPR spectrum through the DNP matching conditions (discussed above), ISE overall produces substantially greater nuclear polarization and superior DNP performance, even though ASE may be more efficient for certain electron spin packets. It should be noted that for very broad EPR spectra, the distinction between ASE and ISE becomes less well-defined, since different spin packets can experience different regimes during the same frequency sweep.

As illustrated in Figure 1d, the optimal SE condition is confined to a narrow frequency window. In practice, for conventional CW DNP, locating the optimal DNP conditions often requires repeated adjustments of the magnetic field or microwave frequency, making the optimization process tedious and time-consuming. Even for the same metal ion, such as Mn^{2+}, variations in the local coordination environment can lead to changes in the EPR spectrum, shifting the optimal irradiation frequency. In contrast, ISE not only provides a much larger DNP enhancement but also maintains nearly optimal performance over a wide range of frequencies, as highlighted in Figure 1d. As a result, chirped DNP is significantly more robust with respect to the experimental parameters and requires considerably less optimization.

Using optimized ISE conditions, a maximum enhancement of $\varepsilon = \varepsilon_{on}/\varepsilon_{off} = 79$ was achieved at 80 K. Panels a and b of Figure 3 show the DNP buildup of Mn-doped LTO at 20 and 80 K, respectively, and the corresponding NMR spectra at 80 K are depicted in Figure 3c. This sensitivity enhancement is significantly larger than those typically reported for the abundant ^{7}Li nuclear spins in CW DNP experiments in similar samples.[36,42,43] Interestingly, a larger DNP enhancement can be achieved at 80 K than at 20 K. The shorter T_{1e} at 80 K (21 μs vs 64 μs at 20 K (see the Supporting Information)) allows a shorter optimal repetition delay (100 μs vs 250 μs), enabling more frequent polarization transfer. Although the ratio between the repetition delay, t_d, and the nuclear T_{1n} is similar at both temperatures, the smaller enhancement at 20 K may result from more pronounced sample heating.

In addition to Mn^{2+} (electron spin $S = 5/2$ and nuclear spin $I = 5/2$), Gd^{3+} ($S = 7/2$, and $I = 0$), which has different electron and nuclear spin quantum numbers, was also investigated. Figure 4b compares the DNP frequency profiles of the Gd-doped LTO sample acquired with different chirp bandwidths at 20 K. The experimental parameters were optimized (Figure 4d–f). Since the effective nutation frequency scales as $\omega_1 \propto \sqrt{S(S+1) - m_S(m_S+1)}$, optimal DNP conditions for Gd^{3+} ($S = 7/2$) can be achieved at a microwave power lower than that for Mn^{2+} ($S = 5/2$), as shown by comparing Figures 4d and 1f.

https://doi.org/10.1021/acs.jpclett.6c02353
J. Phys. Chem. Lett. 2026, 17, 10613−10621

Downloaded from pubs.acs.org/jpclcd/article-pdf/17/37/10613/6838270/acs.jpclett.6c02353.pdf by FLORIDA STATE UNIV user on 02 November 2026

Frequency-swept DNP yields approximately an order-of-magnitude larger DNP enhancement than SE, while maintaining nearly optimal performance over a broad frequency range, as depicted in panels b and c of Figure 4. For Gd^{3+}, the superiority of ISE over ASE is even more pronounced than for Mn^{2+}. Reversing the chirp direction inverts the DNP frequency profile, as shown in Figure 4c and the inset of Figure 4b. This behavior further demonstrates the coherent nature of chirped DNP, in which the electron polarization adiabatically follows the effective magnetic field in the rotating frame (adiabaticity factor $Q_1 \gg 1$ (see below)), as illustrated in Figure 2.

The DNP build-up at 20 K of the Gd-doped LTO sample is shown in Figure 5. A maximum enhancement of $\varepsilon = 35$ was achieved under the optimized ISE conditions, comparable to that of the Mn-doped sample at 20 K (Figure 3a), despite the narrower central transition of Gd^{3+} and the much longer nuclear T_1. This can be explained by a lower than nominal concentration of incorporated Gd dopants, as suggested by the nuclear T_1 and NMR line width (shown in the Supporting Information).

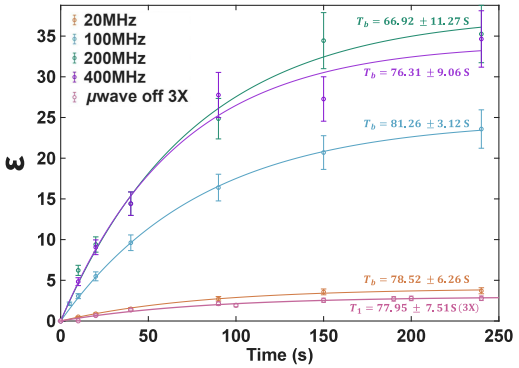


Figure 5. DNP build-up curves of the Gd-doped LTO sample at 20 K. ^{7}Li DNP build-up curves measured using SE and chirped pulses. The solid lines are exponential rise fits. The microwave-off (μwave off) data are multiplied by a factor of 3 for visualization.

For metal-ion DNP, only the central transition (CT), $\left|m_S = -\frac{1}{2}\right\rangle \rightarrow \left|m_S = \frac{1}{2}\right\rangle$, has so far been exploited to polarize nuclear spins because its EPR line is considerably narrower than the satellite transitions (STs). Coherent pulsed DNP provides an additional opportunity to further improve the DNP efficiency by utilizing the satellite transitions of high-spin metal ions. Previous EPR studies have shown that microwave pulses, particularly adiabatic pulses, can efficiently invert the electron populations among the satellite transitions. This increases the population difference between the $\left|m_S = -\frac{1}{2}\right\rangle$ and $\left|m_S = \frac{1}{2}\right\rangle$ states, thereby enhancing the EPR signal of the central transition. For instance, this principle has been exploited in double electron−electron resonance (DEER) experiments to improve sensitivity,[67] and related approaches have also been applied in NMR of quadrupolar nuclei.[68] Here, we employ this enhancement of the CT to improve the efficiency of pulsed DNP.

Both population inversion of the satellite transition and the ASE/ISE DNP process can be described in terms of level anti-crossings using the Landau−Zener formalism.[53] Population inversion of the satellite transition involves a first-order allowed transition, whereas ASE/ISE is mediated by a second-order forbidden transition. Consequently, the efficiencies of the ST inversion and ASE/ISE processes are governed by the corresponding adiabaticity factors

$$Q_1 = \frac{\pi\omega_1^2}{\dot{\omega}_m};\ Q_2 = \frac{2\pi \sin^2\theta M_2}{|\cos\theta\dot{\omega}_m|} \quad (1)$$

where $\dot{\omega}_m$ is the microwave frequency sweep rate, $\sin\theta = \omega_1/\omega_{0I}$, and $M_2 = \frac{1}{2}\sum\left|\frac{1}{4}A_{z+}\right|^2$ the second moment of the nonsecular electron−nuclear dipolar interaction. Detailed derivations can be found in refs 53 and 63.

Efficient ST inversion and ISE require separate optimization of Q_1 and Q_2. The former requires $Q_1 \gg 1$. As a first-order transition, this condition can be readily satisfied, and a rapid frequency sweep is sufficient to achieve nearly complete inversion. Experimentally, the inversion efficiency is charac-

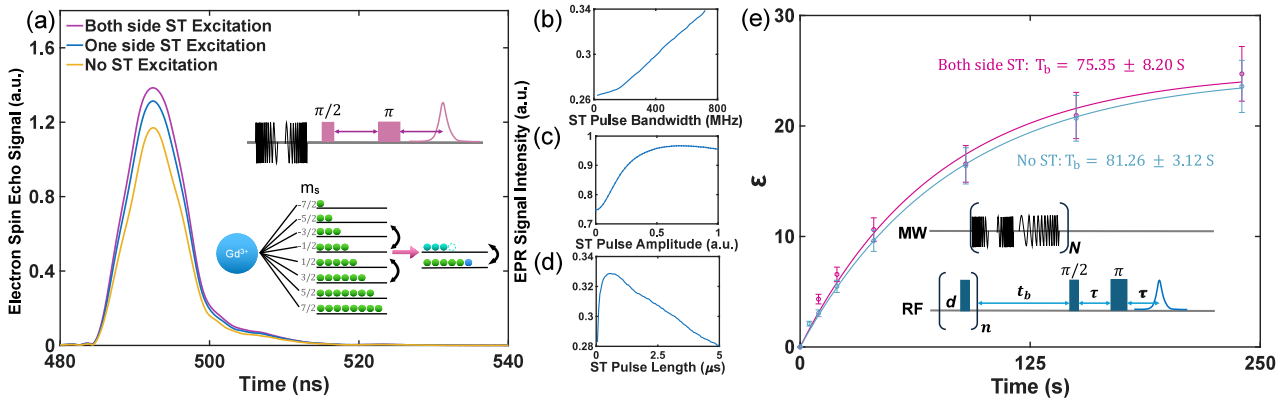


Figure 6. Enhancing EPR and DNP through satellite transition excitation. (a) Electron spin echo signals of the Gd-doped LTO sample detected following selective excitation of the STs on both sides of the EPR spectrum (at 1.1 and 1.97 GHz), on only one side (at 1.1 GHz), or without ST excitation. The inset shows the microwave pulse sequence, in which two frequency-swept pulses with a sweep bandwidth of 630 MHz and a duration of 0.8 μs were applied prior to the Hahn echo measurement. (b−d) Dependence of the electron spin echo intensity on the frequency sweep bandwidth, microwave amplitude, and chirped pulse duration of the ST excitation pulses, respectively. (e) DNP build-up with and without ST excitation. Two rapid chirped pulses sweeping 600 MHz in 0.8 μs were applied before a 10 μs DNP chirped pulse sweeping 100 MHz and compared with a single 12 μs DNP chirped pulse sweeping 100 MHz.

Downloaded from pubs.acs.org/jpclcd/article-pdf/17/37/10613/6838270/acs.jpclett.6c02353.pdf by FLORIDA STATE UNIV user on 02 November 2026

https://doi.org/10.1021/acs.jpclett.6c02353
J. Phys. Chem. Lett. 2026, 17, 10613−10621

terized by measuring the Hahn echo intensity after the ST excitation pulses, as illustrated in Figure 6. A relatively short (<1 μs) pulse (large $\dot{\omega}_m$) is sufficient to maximize the echo intensity. The nutation frequency is approximately $\omega_1/2\pi \sim 50$ MHz, and sweeping a 1 GHz bandwidth in 1 μs yields $Q_1 \sim 50$, ensuring adiabaticity. Interestingly, the echo intensity decreases for pulses longer than ~1 μs. This behavior was also observed by Doll et al.[67] and was attributed to (i) sample heating due to the pulses and (ii) pulse distortions resulting in unwanted excitation of the spins to be polarized. However, we observe only a ~12% increase in the EPR echo intensity following ST excitations. This modest enhancement is primarily limited by the bandwidth of the EIK (~1 GHz), which is sufficient to excite only a small fraction of the Gd^{3+} STs, whose STs span more than 20 GHz (Figure 4a). In principle, a broader chirp would enable population inversion of all STs, thereby exchanging the populations of the outer spin states with the $\left|m_S = \pm\frac{1}{2}\right\rangle$ states. In this ideal case, the population difference for the CT can be enhanced by a factor of 7 for $S = 7/2$ Gd^{3+}, significantly exceeding the thermal electron polarization limit.

In contrast to ST inversion, satisfying the optimal condition for ISE ($Q_2 \sim \sqrt{2}/2$)[53] is considerably more challenging at high magnetic fields due to the nature of the second-order forbidden transition. The dependence of the DNP enhancement on the ISE pulse duration is shown in Figure 6a, indicating that a slower frequency sweep is required to satisfy the adiabaticity condition. To estimate the adiabaticity, we take $\omega_1/2\pi = 50$ MHz, $\sqrt{M_2} \sim 0.15$ MHz, and a 100 MHz chirp over 10 μs, yielding $Q_2 \sim 1.1$,[53] which is close to the optimal adiabaticity condition. We therefore apply the following pulse scheme. Two rapid chirped pulses first invert the populations of the STs enhancing the CT, followed by a slower ISE chirped pulse that transfers the enhanced central transition electron polarization to the nuclear spins. Compared with the sequence without the satellite transition excitation pulses, this approach yields an approximately 5% improvement, as shown in Figure 6e. This improvement is smaller than the 12% enhancement observed in the EPR signal, likely due to additional limitations by nuclear T_1 relaxation during the polarization buildup and inefficient ^{7}Li spin diffusion.

Another important factor that has not yet been discussed, but is crucial for DNP, is the electron spin coherence time.[64] In conventional CW DNP, the polarization transfer efficiency is often limited by the short electron spin coherence time, T_{2e}. This is also one of the reasons why DNP generally performs better at low temperatures, where T_{2e} is significantly prolonged. In contrast, coherent pulsed DNP can extend the effective coherence time by more than an order of magnitude. For example, in frequency-swept DNP, the relevant coherence is governed by the $T_{1\rho}$ in the rotating frame, rather than T_{2e}, and $T_{1\rho}$ is typically much longer. This advantage is particularly significant for metal-ion DNP, where the electron spin coherence times of metal centers are generally much shorter than those of organic radicals. Therefore, beyond the advantages discussed above, the prolonged coherence time by microwave pulses can further enhance DNP. More broadly, this capability may enable efficient pulsed DNP at much higher temperatures, potentially even approaching room temperature.

In summary, we present the first experimental demonstration of coherent pulsed endogenous metal-ion DNP at W-band using the HiPER spectrometer. For Mn-doped LTO, we achieved a maximum DNP enhancement of $\varepsilon = 79$ for abundant ^{7}Li using ISE at 3.364 T and 80 K, substantially exceeding the values previously reported for similar samples with the same metal center concentration.[25,36,42,43] Unlike using narrow-line radicals, for which ASE is typically the most efficient DNP scheme, ISE is more efficient for metal ions with a broad EPR line. Compared with conventional single-frequency SE, ISE improves the DNP enhancement by factors of approximately 3 for Mn^{2+} and approximately 10 for Gd^{3+} under the same microwave power. This improvement is substantially greater than that reported for radical-based DNP systems[54] and is primarily attributed to the EPR line width of the paramagnetic metal ions being much broader than the nuclear Larmor frequency. These results highlight the fact that metal-ion DNP is expected to benefit more than radical-based DNP from the advancement of coherent pulsed DNP methods. In addition, coherent frequency-swept DNP is highly robust, maintaining nearly optimal performance over a broad range of microwave frequencies and experimental parameters, which simplifies experimental optimization. Interestingly, Mn-doped LTO exhibits higher DNP efficiency at 80 K than at 20 K because of the shorter electron T_{1e}.

Additionally, we demonstrate the concept of using adiabatic inversion pulses to selectively excite the satellite transitions and thereby enhance the polarization of the central transition in high-spin systems, which is then exploited for DNP. This approach is expected to become significantly more effective with the development of broadband microwave amplifiers, such as traveling-wave tube (TWT) amplifiers.[69]

Despite significant progress, the development of pulsed DNP is still at an early stage and has thus far been demonstrated primarily at the X- and Q-bands using organic radicals. Our results at the W-band provide compelling evidence that coherent pulsed DNP is a promising strategy for endogenous metal-ion DNP. Endogenous metal-ion DNP holds great promise for applications in materials science, inorganic chemistry, and metalloprotein research. However, the relatively small CW DNP enhancements compared to the values achieved with radicals have limited their broader application. These small enhancements arise from the broad EPR spectra and unfavorable electron spin relaxation properties of the paramagnetic metal centers. We demonstrate that coherent pulsed DNP can overcome these key limitations and substantially improve the DNP efficiency and robustness.

We anticipate that these advances, particularly when combined with MAS NMR, will enable a broad range of material studies that are currently beyond reach. For example, they could facilitate the high-sensitivity detection and characterization of low-abundance quadrupolar nuclei such as ^{17}O,[36,39] enable inherently insensitive techniques such as multiple-quantum magic-angle spinning (MQMAS),[70,71] and enhance the sensitivity of multidimensional NMR experiments for the structural characterization of complex materials. Continued advances in high-field pulsed DNP instrumentation and methodology will be essential to realizing the potential of these approaches.

■ ASSOCIATED CONTENT

Supporting Information

The Supporting Information is available free of charge at https://pubs.acs.org/doi/10.1021/acs.jpclett.6c02353.

Downloaded from pubs.acs.org/jpclcd/article-pdf/17/37/10613/6838270/acs.jpclett.6c02353.pdf by FLORIDA STATE UNIV user on 02 November 2026

https://doi.org/10.1021/acs.jpclett.6c02353
J. Phys. Chem. Lett. 2026, 17, 10613−10621

Sample preparation (section I), sample characterization, including powder X-ray diffraction, scanning electron microscopy, solid-state NMR, and W-band EPR (section II), and W-band DNP NMR measurements on the HiPER (section III) (PDF)

AUTHOR INFORMATION

Corresponding Author

Yifan Quan − *Department of Chemistry, University of Pennsylvania, Philadelphia, Pennsylvania 19104, United States;* orcid.org/0000-0001-8632-9437; Email: yquan@sas.upenn.edu

Authors

Liangping Zhu − *Department of Chemistry, University of Pennsylvania, Philadelphia, Pennsylvania 19104, United States;* orcid.org/0009-0007-2964-591X

Duhan Zhang − *Department of Chemistry, University of Pennsylvania, Philadelphia, Pennsylvania 19104, United States;* orcid.org/0000-0001-9428-956X

Haoyu Liu − *Department of Chemistry, University of Pennsylvania, Philadelphia, Pennsylvania 19104, United States*

Ashley N. Beers − *Department of Chemistry, University of Pennsylvania, Philadelphia, Pennsylvania 19104, United States*

Yunfan Qiu − *Department of Chemistry and Biochemistry, Utah State University, Logan, Utah 84322, United States;* orcid.org/0000-0002-4666-1424

Thierry Dubroca − *National High Magnetic Field Laboratory, Tallahassee, Florida 32310, United States*

Complete contact information is available at: https://pubs.acs.org/10.1021/acs.jpclett.6c02353

Notes

The authors declare no competing financial interest.

ACKNOWLEDGMENTS

The authors thank Michal Leskes for her invaluable discussion, Samuel Veroneau, Inabat Khamitova, Matthew Mena, Anna Lisa, and Miranda Wright for assistance with sample synthesis, and Manoj Subramanya for sample characterization. EPR and DNP were performed at the National High Magnetic Field Laboratory, which is supported in part by the National Science Foundation (Grant DMR-2128556) and the State of Florida. The authors acknowledge the design and fabrication of one of the RF circuits used in the DNP experiments by Raquel Marriott, Korrigan Amadi, Ty Chiasson, Christopher Balthazar, Christian Hurdis, and Dylan Joerder. The samples were characterized at the XRD (NSF Grant DMR-2309043) and SEM (NSF Grant NNCI-2025608) facilities at the University of Pennsylvania.

REFERENCES

(1) Maly, T.; Debelouchina, G. T.; Bajaj, V. S.; Hu, K. N.; Joo, C. G.; Mak-Jurkauskas, M. L.; Sirigiri, J. R.; van der Wel, P. C. A.; Herzfeld, J.; Temkin, R. J.; Griffin, R. G. Dynamic nuclear polarization at high magnetic fields. *J. Chem. Phys.* **2008**, *128*, 052211.

(2) Barnes, A. B.; De Paëpe, G.; van der Wel, P. C.; Hu, K. N.; Joo, C. G.; Bajaj, V. S.; Mak-Jurkauskas, M. L.; Sirigiri, J. R.; Herzfeld, J.; Temkin, R. J.; Griffin, R. G. High-Field Dynamic Nuclear Polarization for Solid and Solution Biological NMR. *Appl. Magn. Reson.* **2008**, *34*, 237−263.

(3) Eills, J.; Budker, D.; Cavagnero, S.; Chekmenev, E. Y.; Elliott, S. J.; Jannin, S.; Lesage, A.; Matysik, J.; Meersmann, T.; Prisner, T.; Reimer, J. A.; Yang, H.; Koptyug, I. V. Spin Hyperpolarization in Modern Magnetic Resonance. *Chem. Rev.* **2023**, *123*, 1417−1551.

(4) Bajaj, V. S.; Mak-Jurkauskas, M. L.; Belenky, M.; Herzfeld, J.; Griffin, R. G. Functional and shunt states of bacteriorhodopsin resolved by 250 GHz dynamic nuclear polarization−enhanced solid-state NMR. *Proc. Natl. Acad. Sci. U. S. A.* **2009**, *106*, 9244−9249.

(5) Debelouchina, G. T.; Bayro, M. J.; van der Wel, P. C.; Caporini, M. A.; Barnes, A. B.; Rosay, M.; Maas, W. E.; Griffin, R. G. Dynamic nuclear polarization-enhanced solid-state NMR spectroscopy of GNNQQNY nanocrystals and amyloid fibrils. *Physical Chemistry Chemical Physics* **2010**, *12*, 5911−9.

(6) Debelouchina, G. T.; Bayro, M. J.; Fitzpatrick, A. W.; Ladizhansky, V.; Colvin, M. T.; Caporini, M. A.; Jaroniec, C. P.; Bajaj, V. S.; Rosay, M.; Macphee, C. E.; Vendruscolo, M.; Maas, W. E.; Dobson, C. M.; Griffin, R. G. Higher order amyloid fibril structure by MAS NMR and DNP spectroscopy. *J. Am. Chem. Soc.* **2013**, *135*, 19237−47.

(7) Ni, Q. Z.; Can, T. V.; Daviso, E.; Belenky, M.; Griffin, R. G.; Herzfeld, J. Primary Transfer Step in the Light-Driven Ion Pump Bacteriorhodopsin: An Irreversible U-Turn Revealed by Dynamic Nuclear Polarization-Enhanced Magic Angle Spinning NMR. *J. Am. Chem. Soc.* **2018**, *140*, 4085−4091.

(8) Becker-Baldus, J.; Bamann, C.; Saxena, K.; Gustmann, H.; Brown, L. J.; Brown, R. C. D.; Reiter, C.; Bamberg, E.; Wachtveitl, J.; Schwalbe, H.; Glaubitz, C. Enlightening the photoactive site of channelrhodopsin-2 by DNP-enhanced solid-state NMR spectroscopy. *Proc. Natl. Acad. Sci. U. S. A.* **2015**, *112*, 9896−9901.

(9) Mehler, M.; Eckert, C. E.; Leeder, A. J.; Kaur, J.; Fischer, T.; Kubatova, N.; Brown, L. J.; Brown, R. C. D.; Becker-Baldus, J.; Wachtveitl, J.; Glaubitz, C. Chromophore Distortions in Photointermediates of Proteorhodopsin Visualized by Dynamic Nuclear Polarization-Enhanced Solid-State NMR. *J. Am. Chem. Soc.* **2017**, *139*, 16143−16153.

(10) Joedicke, L.; Mao, J.; Kuenze, G.; Reinhart, C.; Kalavacherla, T.; Jonker, H. R. A.; Richter, C.; Schwalbe, H.; Meiler, J.; Preu, J.; Michel, H.; Glaubitz, C. The molecular basis of subtype selectivity of human kinin G-protein-coupled receptors. *Nat. Chem. Biol.* **2018**, *14*, 284−290.

(11) Albert, B. J.; Gao, C.; Sesti, E. L.; Saliba, E. P.; Alaniva, N.; Scott, F. J.; Sigurdsson, S. T.; Barnes, A. B. Dynamic Nuclear Polarization Nuclear Magnetic Resonance in Human Cells Using Fluorescent Polarizing Agents. *Biochemistry* **2018**, *57*, 4741−4746.

(12) Maciejko, J.; Mehler, M.; Kaur, J.; Lieblein, T.; Morgner, N.; Ouari, O.; Tordo, P.; Becker-Baldus, J.; Glaubitz, C. Visualizing Specific Cross-Protomer Interactions in the Homo-Oligomeric Membrane Protein Proteorhodopsin by Dynamic-Nuclear-Polarization-Enhanced Solid-State NMR. *J. Am. Chem. Soc.* **2015**, *137*, 9032−9043.

(13) Haber, S.; Rosy; Saha, A.; Brontvein, O.; Carmieli, R.; Zohar, A.; Noked, M.; Leskes, M. Structure and Functionality of an Alkylated LixSiyOz Interphase for High-Energy Cathodes from DNP-ssNMR Spectroscopy. *J. Am. Chem. Soc.* **2021**, *143*, 4694−4704.

(14) Bahri, S.; Silvers, R.; Michael, B.; Jaudzems, K.; Lalli, D.; Casano, G.; Ouari, O.; Lesage, A.; Pintacuda, G.; Linse, S.; Griffin, R. G. ^{1}H detection and dynamic nuclear polarization enhanced NMR of $A\beta_{1-42}$ fibrils. *Proc. Natl. Acad. Sci. U. S. A.* **2022**, *119*, e2114413119.

(15) Jeon, J.; Blake Wilson, C.; Yau, W. M.; Thurber, K. R.; Tycko, R. Time-resolved solid state NMR of biomolecular processes with millisecond time resolution. *Journal of Magnetic Resonance* **2022**, *342*, 107285.

(16) Movellan, K. T.; Zhu, W.; Banks, D.; Kempf, J.; Runge, B.; Gronenborn, A. M.; Polenova, T. Expanding the tool box for native structural biology: 19F dynamic nuclear polarization with fast magic angle spinning. *Sci. Adv.* **2024**, *10*, eadq3115.

Downloaded from pubs.acs.org/jpclcod/article-pdf/17/37/10613/6838270/acs.jpclett.6c02353.pdf by FLORIDA STATE UNIV user on 02 November 2026

(17) Krafcikova, M. D.; Beriashvili, D.; Bahri, S.; Bergmeijer, M.; Howes, S. C.; Gurinov, A.; Forster, F. G.; Folkers, G. E.; Baldus, M. A DNP-Supported Solid-State NMR Approach to Study Nucleic Acids In Situ Reveals Berberine-Stabilized Hoogsteen Structures in Mitochondria. *Angew. Chem., Int. Ed.* **2025**, *64*, e202424131.
(18) Lesage, A.; Lelli, M.; Gajan, D.; Caporini, M. A.; Vitzthum, V.; Miéville, P.; Alauzun, J.; Roussey, A.; Thieuleux, C.; Mehdi, A.; Bodenhausen, G.; Coperet, C.; Emsley, L. Surface Enhanced NMR Spectroscopy by Dynamic Nuclear Polarization. *J. Am. Chem. Soc.* **2010**, *132*, 15459−15461.
(19) Piveteau, L.; Ong, T. C.; Rossini, A. J.; Emsley, L.; Coperet, C.; Kovalenko, M. V. Structure of Colloidal Quantum Dots from Dynamic Nuclear Polarization Surface Enhanced NMR Spectroscopy. *J. Am. Chem. Soc.* **2015**, *137*, 13964−71.
(20) Rej, E.; Gaebel, T.; Waddington, D. E. J.; Reilly, D. J. Hyperpolarized Nanodiamond Surfaces. *J. Am. Chem. Soc.* **2017**, *139*, 193−199.
(21) Berruyer, P.; Emsley, L.; Lesage, A. DNP in Materials Science: Touching the Surface. *eMagRes* **2018**, 93−104.
(22) Azaïs, T.; Von Euw, S.; Ajili, W.; Auzoux-Bordenave, S.; Bertani, P.; Gajan, D.; Emsley, L.; Nassif, N.; Lesage, A. Structural description of surfaces and interfaces in biominerals by DNP SENS. *Solid State Nuclear Magnetic Resonance* **2019**, *102*, 2−11.
(23) Kubicki, D. J.; Stranks, S. D.; Grey, C. P.; Emsley, L. NMR spectroscopy probes microstructure, dynamics and doping of metal halide perovskites. *Nature Reviews Chemistry* **2021**, *5*, 624−645.
(24) Jardon-Alvarez, D.; Leskes, M. Metal ions based dynamic nuclear polarization: MI-DNP. *Progress in Nuclear Magnetic Resonance Spectroscopy* **2023**, *138-139*, 70−104.
(25) Karmakar, A.; Bernard, G. M.; Pominov, A.; Tabassum, T.; Chaklashiya, R.; Han, S.; Jain, S. K.; Michaelis, V. K. Triangulating Dopant-Level Mn(II) Insertion in a Cs(2)NaBiCl(6) Double Perovskite Using Magnetic Resonance Spectroscopy. *J. Am. Chem. Soc.* **2023**, *145*, 4485−4499.
(26) Sarkar, D.; Stelmakh, A.; Karmakar, A.; Aebli, M.; Krieg, F.; Bhattacharya, A.; Pawsey, S.; Kovalenko, M. V.; Michaelis, V. K. Surface Structure of Lecithin-Capped Cesium Lead Halide Perovskite Nanocrystals Using Solid-State and Dynamic Nuclear Polarization NMR Spectroscopy. *ACS Nano* **2024**, *18*, 21894−21910.
(27) Maity, A.; Svirinovsky-Arbeli, A.; Buganim, Y.; Oppenheim, C.; Leskes, M. Tracking dendrites and solid electrolyte interphase formation with dynamic nuclear polarization-NMR spectroscopy. *Nat. Commun.* **2024**, *15*, 9956.
(28) Steinberg, Y.; Sebti, E.; Moroz, I. B.; Zohar, A.; Jardon-Alvarez, D.; Bendikov, T.; Maity, A.; Carmieli, R.; Clement, R. J.; Leskes, M. Composition and Structure of the solid electrolyte interphase on Na-Ion Anodes Revealed by Exo- and Endogenous Dynamic Nuclear Polarization horizontal line NMR Spectroscopy. *J. Am. Chem. Soc.* **2024**, *146*, 24476−24492.
(29) Abutbul, R. E.; Jardon-Alvarez, D.; Houben, L.; Golani, O.; Sivan, E.; Carmieli, R.; Kaminker, I.; Leskes, M. Metal Ion Dynamic Nuclear Polarization in Mn(II)-Doped CdS Nanocrystals: Atomic-Scale Investigation of the Dopant and Its Host. *ACS Nano* **2025**, *19*, 17640−17652.
(30) Ardenkjaer-Larsen, J. H.; Fridlund, B.; Gram, A.; Hansson, G.; Hansson, L.; Lerche, M. H.; Servin, R.; Thaning, M.; Golman, K. Increase in signal-to-noise ratio of > 10,000 times in liquid-state NMR. *Proc. Natl. Acad. Sci. U. S. A.* **2003**, *100*, 10158−10163.
(31) Ardenkjaer-Larsen, J. H. On the present and future of dissolution-DNP. *Journal of Magnetic Resonance* **2016**, *264*, 3−12.
(32) Pinon, A. C.; Capozzi, A.; Ardenkjaer-Larsen, J. H. Hyperpolarization via dissolution dynamic nuclear polarization: new technological and methodological advances. *Magnetic Resonance Materials in Physics, Biology and Medicine* **2021**, *34*, 5−23.
(33) Rossini, A. J.; Zagdoun, A.; Lelli, M.; Lesage, A.; Copéret, C.; Emsley, L. Dynamic Nuclear Polarization Surface Enhanced NMR Spectroscopy. *Acc. Chem. Res.* **2013**, *46*, 1942−1951.
(34) Mishra, A.; Hope, M. A.; Stevanato, G.; Kubicki, D. J.; Emsley, L. Dynamic Nuclear Polarization of Inorganic Halide Perovskites. *J. Phys. Chem. C* **2023**, *127*, 11094−11102.
(35) Corzilius, B.; Smith, A. A.; Barnes, A. B.; Luchinat, C.; Bertini, I.; Griffin, R. G. High-Field Dynamic Nuclear Polarization with High-Spin Transition Metal Ions. *J. Am. Chem. Soc.* **2011**, *133*, 5648−5651.
(36) Wolf, T.; Kumar, S.; Singh, H.; Chakrabarty, T.; Aussenac, F.; Frenkel, A. I.; Major, D. T.; Leskes, M. Endogenous Dynamic Nuclear Polarization for Natural Abundance (17)O and Lithium NMR in the Bulk of Inorganic Solids. *J. Am. Chem. Soc.* **2019**, *141*, 451−462.
(37) Hope, M. A.; Björgvinsdóttir, S.; Halat, D. M.; Menzildjian, G.; Wang, Z.; Zhang, B.; MacManus-Driscoll, J. L.; Lesage, A.; Lelli, M.; Emsley, L.; Grey, C. P. Endogenous 17O Dynamic Nuclear Polarization of Gd-Doped CeO2 from 100 to 370 K. *J. Phys. Chem. C* **2021**, *125*, 18799−18809.
(38) Rao, Y.; Palumbo, C. T.; Venkatesh, A.; Keener, M.; Stevanato, G.; Chauvin, A.-S.; Menzildjian, G.; Kuzin, S.; Yulikov, M.; Jeschke, G.; Lesage, A.; Mazzanti, M.; Emsley, L. Design Principles for the Development of Gd(III) Polarizing Agents for Magic Angle Spinning Dynamic Nuclear Polarization. *J. Phys. Chem. C* **2022**, *126*, 11310−11317.
(39) Jardon-Alvarez, D.; Reuveni, G.; Harchol, A.; Leskes, M. Enabling Natural Abundance (17)O Solid-State NMR by Direct Polarization from Paramagnetic Metal Ions. *J. Phys. Chem. Lett.* **2020**, *11*, 5439−5445.
(40) Hope, M. A.; Björgvinsdóttir, S.; Grey, C. P.; Emsley, L. A Magic Angle Spinning Activated 17O DNP Raser. *J. Phys. Chem. Lett.* **2021**, *12*, 345−349.
(41) Moroz, I. B.; Feldman, Y.; Carmieli, R.; Liu, X.; Leskes, M. Endogenous metal-ion dynamic nuclear polarization for NMR signal enhancement in metal organic frameworks. *Chemical Science* **2024**, *15*, 336−348.
(42) Chakrabarty, T.; Goldin, N.; Feintuch, A.; Houben, L.; Leskes, M. Paramagnetic Metal-Ion Dopants as Polarization Agents for Dynamic Nuclear Polarization NMR Spectroscopy in Inorganic Solids. *ChemPhysChem* **2018**, *19*, 2139−2142.
(43) Livni, N.; Paul, S.; Moroz, I. B.; Bogdanov, A. V.; Jardon-Alvarez, D.; Mentink-Vigier, F.; Leskes, M. Isotropic Hyperfine Interactions Drive Cross-Effect Dynamic Nuclear Polarization. *J. Phys. Chem. Lett.* **2025**, *16*, 11955−11963.
(44) Eichhorn, T. R.; Haag, M.; van den Brandt, B.; Hautle, P.; Wenckebach, W. T. High proton spin polarization with DNP using the triplet state of pentacene-d14. *Chemical Physics Letters* **2013**, *555*, 296−299.
(45) Eichhorn, T. R.; Brandt, B. v. d.; Hautle, P.; Henstra, A.; Wenckebach, W. T. Dynamic nuclear polarisation via the integrated solid effect II: experiments on naphthalene-h8 doped with pentacene-d14. *Molecular Physics* **2014**, *112*, 1773−1782.
(46) Henstra, A.; Wenckebach, W. The theory of nuclear orientation via electron spin locking (NOVEL). *Molecular Physics* **2008**, *106*, 859−871.
(47) Can, T. V.; Walish, J. J.; Swager, T. M.; Griffin, R. G. Time domain DNP with the NOVEL sequence. *J. Chem. Phys.* **2015**, *143*, 054201.
(48) Can, T. V.; Weber, R. T.; Walish, J. J.; Swager, T. M.; Griffin, R. G. Ramped-amplitude NOVEL. *J. Chem. Phys.* **2017**, *146*, 154204.
(49) Jain, S. K.; Mathies, G.; Griffin, R. G. Off-resonance NOVEL. *J. Chem. Phys.* **2017**, *147*, 164201.
(50) Can, T. V.; McKay, J. E.; Weber, R. T.; Yang, C.; Dubroca, T.; van Tol, J.; Hill, S.; Griffin, R. G. Frequency-Swept Integrated and Stretched Solid Effect Dynamic Nuclear Polarization. *J. Phys. Chem. Lett.* **2018**, *9*, 3187−3192.
(51) Tan, K. O.; Yang, C.; Weber, R. T.; Mathies, G.; Griffin, R. G. Time-optimized pulsed dynamic nuclear polarization. *Sci. Adv.* **2019**, *5*, eaav6909.
(52) Redrouthu, V. S.; Mathies, G. Efficient Pulsed Dynamic Nuclear Polarization with the X-Inverse-X Sequence. *J. Am. Chem. Soc.* **2022**, *144*, 1513−1516.

Downloaded from pubs.acs.org/jpclcd/article-pdf/17/37/10613/6838270/acs.jpclett.6c02353.pdf by FLORIDA STATE UNIV user on 02 November 2026

https://doi.org/10.1021/acs.jpclett.6c02353
J. Phys. Chem. Lett. 2026, 17, 10613−10621

(53) Quan, Y.; Steiner, J.; Ouyang, Y.; Tan, K. O.; Wenckebach, W. T.; Hautle, P.; Griffin, R. G. Integrated, Stretched, and Adiabatic Solid Effects. *J. Phys. Chem. Lett.* **2022**, *13*, 5751−5757.
(54) Quan, Y.; Subramanya, M. V. H.; Ouyang, Y.; Mardini, M.; Dubroca, T.; Hill, S.; Griffin, R. G. Coherent Dynamic Nuclear Polarization using Chirped Pulses. *J. Phys. Chem. Lett.* **2023**, *14*, 4748−4753.
(55) Zhao, Y.; El Mkami, H.; Hunter, R. I.; Casano, G.; Ouari, O.; Smith, G. M. Large cross-effect dynamic nuclear polarisation enhancements with kilowatt inverting chirped pulses at 94 GHz. *Commun. Chem.* **2023**, *6*, 171.
(56) Redrouthu, V. S.; Vinod-Kumar, S.; Mathies, G. Dynamic nuclear polarization by two-pulse phase modulation. *J. Chem. Phys.* **2023**, *159*, 014201.
(57) Camenisch, G. M.; Wili, N.; Jeschke, G.; Ernst, M. Pulsed dynamic nuclear polarization: a comprehensive Floquet description. *Physical Chemistry Chemical Physics* **2024**, *26*, 17666−17683.
(58) Zhang, Q.; Verde, M. G.; Seo, J. K.; Li, X.; Meng, Y. S. Structural and electrochemical properties of Gd-doped Li4Ti5O12 as anode material with improved rate capability for lithium-ion batteries. *J. Power Sources* **2015**, *280*, 355−362.
(59) Cruickshank, P. A. S.; Bolton, D. R.; Robertson, D. A.; Hunter, R. I.; Wylde, R. J.; Smith, G. M. A kilowatt pulsed 94 GHz electron paramagnetic resonance spectrometer with high concentration sensitivity, high instantaneous bandwidth, and low dead time. *Rev. Sci. Instrum.* **2009**, *80*, 103102.
(60) Hunter, R. I.; Cruickshank, P. A. S.; Bolton, D. R.; Riedi, P. C.; Smith, G. M. High power pulsed dynamic nuclear polarisation at 94 GHz. *Physical Chemistry Chemical Physics* **2010**, *12*, 5752−5756.
(61) Subramanya, M. V. H.; Marbey, J.; Kundu, K.; McKay, J. E.; Hill, S. Broadband Fourier-Transform-Detected EPR at W-Band. *Applied Magnetic Resonance* **2023**, *54*, 165−181.
(62) Epel, B.; Gromov, I.; Stoll, S.; Schweiger, A.; Goldfarb, D. Spectrometer manager: A versatile control software for pulse EPR spectrometers. *Concepts in Magnetic Resonance Part B: Magnetic Resonance Engineering* **2005**, *26B*, 36−45.
(63) Henstra, A.; Wenckebach, W. T. Dynamic nuclear polarisation via the integrated solid effect I: theory. *Molecular Physics* **2014**, *112*, 1761−1772.
(64) Jhamnani, M.; Sadasivan, S. V.; Jain, S. K.; Equbal, A. Role of quantum coherence in chirped dynamic nuclear polarization. *J. Chem. Phys.* **2025**, *163*, 034203.
(65) Henstra, A.; Dirksen, P.; Schmidt, J.; Wenckebach, W. T. Nuclear spin orientation via electron spin locking (NOVEL). *J. Magn. Reson. (1969-1992)* **1988**, *77*, 389−393.
(66) Tan, K. O.; Weber, R. T.; Can, T. V.; Griffin, R. G. Adiabatic Solid Effect. *J. Phys. Chem. Lett.* **2020**, *11*, 3416−3421.
(67) Doll, A.; Qi, M.; Pribitzer, S.; Wili, N.; Yulikov, M.; Godt, A.; Jeschke, G. Sensitivity enhancement by population transfer in Gd(iii) spin labels. *Physical Chemistry Chemical Physics* **2015**, *17*, 7334−7344.
(68) Hung, I.; Gan, Z. Isotropic solid-state MQMAS NMR spectra for large quadrupolar interactions using satellite-transition selective inversion pulses and low rf fields. *Journal of Magnetic Resonance* **2021**, *324*, 106913.
(69) Pan, P.; Zheng, Y.; Li, Y.; Song, X.; Feng, Z.; Feng, J.; Britt, R. D.; Luhmann, N. C. Demonstration of a 263-GHz Traveling Wave Tube for Electron Paramagnetic Resonance Spectroscopy. *IEEE Transactions on Electron Devices* **2023**, *70*, 5897−5902.
(70) Medek, A.; Harwood, J. S.; Frydman, L. Multiple-Quantum Magic-Angle Spinning NMR: A New Method for the Study of Quadrupolar Nuclei in Solids. *J. Am. Chem. Soc.* **1995**, *117*, 12779−12787.
(71) Hung, I.; Keeler, E. G.; Mao, W.; Gor'kov, P. L.; Griffin, R. G.; Gan, Z. Residue-Specific High-Resolution (17)O Solid-State Nuclear Magnetic Resonance of Peptides: Multidimensional Indirect (1)H Detection and Magic-Angle Spinning. *J. Phys. Chem. Lett.* **2022**, *13*, 6549−6558.

Downloaded from pubs.acs.org/jpclcd/article-pdf/17/37/10613/6838270/acs.jpclett.6c02353.pdf by FLORIDA STATE UNIV user on 02 November 2026

https://doi.org/10.1021/acs.jpclett.6c02353
J. Phys. Chem. Lett. 2026, 17, 10613−10621